An orbital angular momentum radio communication system optimized by intensity controlled masks effectively: Theoretical design and experimental verification

Xinlu Gao,[1,2] Shanguo Huang,[1,a)] Yongfeng Wei,[1] Wensheng Zhai,[1] Wenjing Xu,[1] Shan Yin,[1] Jing Zhou,[2] and Wanyi Gu[1]
[1]*State Key Laboratory of Information Photonics and Optical Communications, Beijing University of Posts and Telecommunications, Beijing 100876, China*
[2]*Applied Optics Beijing Area Major Laboratory, Department of Physics, Beijing Normal University, Beijing 100875, China*

(Received 19 September 2014; accepted 2 December 2014; published online 17 December 2014)

A system of generating and receiving orbital angular momentum (OAM) radio beams, which are collectively formed by two circular array antennas (CAAs) and effectively optimized by two intensity controlled masks, is proposed and experimentally investigated. The scheme is effective in blocking of the unwanted OAM modes and enhancing the power of received radio signals, which results in the capacity gain of system and extended transmission distance of the OAM radio beams. The operation principle of the intensity controlled masks, which can be regarded as both collimator and filter, is feasible and simple to realize. Numerical simulations of intensity and phase distributions at each key cross-sectional plane of the radio beams demonstrate the collimated results. The experimental results match well with the theoretical analysis and the receive distance of the OAM radio beam at radio frequency (RF) 20 GHz is extended up to 200 times of the wavelength of the RF signals, the measured distance is 5 times of the original measured distance. The presented proof-of-concept experiment demonstrates the feasibility of the system. © *2014 AIP Publishing LLC*. [http://dx.doi.org/10.1063/1.4904090]

Electromagnetic (EM) angular momentum as one of the most fundamental physical quantities can be divided into spin angular momentum (SAM) and orbital angular momentum (OAM) in paraxial beams, in both classical and quantum mechanics.[1,2] SAM is associated with photon spin and expressed as circular polarization, and OAM is linked to the spatial distribution in contrast. EM beams carrying OAM can be described in the spatial azimuthal phase term $\exp(il\varphi)(l = 0, \pm1, \pm2...)$, in which φ refers to the azimuth angle and l determines the topological charge of the OAM mode. Moreover, the OAM EM beams have a helical phase front and a "doughnut" intensity shape when the topological charge is nonzero value. In other words, the OAM is a phase singularity nested within the cross-sectional profile of a coherent paraxial beam. And they lie within an unbounded mode space with each mode orthogonal to all of the others.

Nowadays, the orthogonal characteristic has been applied in free-space communication as a new degree of freedom,[3] and this kind of applications has achieved an increase in capacity and spectral efficiency, and data exchange between OAM beams for flexible data processing in 2012.[4] Furthermore, in recent years some excellent works have been done for extending and improving the OAM-based free space optical communication system and suggest that the efficient multiplexing of the independent data-carrying OAM EM beams could be regarded as a possible approach for vastly increasing system capacity and spectral efficiency.[5–8] The basic physical properties of the EM fields can be translated from optics to radio and the OAM radio beams are more immune to atmospheric turbulence interference.[7] Thus, the OAM modes are considered for wireless communications.

Hitherto, there are two methods to generate the radio OAM beams. One method, with the advantage of employing a commercial antenna as the source, is that the radio beam passed through or reflected off a phase mask to get the spatial azimuthal phase distribution, which is corresponded to specific OAM modes.[9,10] Moreover the results from outdoor experiments prove that it is physically feasible to simultaneously transmit different radio frequency (RF) signals with different OAM modes into the far zone and to identify these states, with stirring up some huge repercussion both positive and negative when standard linear momentum antennas are used.[11,12] The other method is based on circular array antennas (CAAs), and some comprehensive system simulations of OAM radio beams were performed.[13,14] In consideration of the method should being flexible, tunable, and reconfigurable, the employing CAAs is more suitable for the requirements of the multiplexing. An OAM-based wireless communication system employing CAAs together with a true time delay (OTTD) unit has been proposed,[15] with the advancements of OTTD contrasted with the traditional electrical phase-shifter such as low loss, small size, lightweight, and immunity to electromagnetic interference.[16] Thanks to the rapidly developing OTTD technology,[17–19] the CAA-generated OAM radio beams are experimentally achieved but the beams just transmit at a short distance of 75 cm, which is equal to 50 times of the signals wavelength.[20,21] Thus, some problems of the OAM radio beams generated by

a)Author to whom correspondence should be addressed. Electronic mail: shghuang@bupt.edu.cn.

uniform CAAs in the transmission and reception need to be solved.

In this paper, an overview of the above transmission and reception problems and an effective solution are proposed and experimentally demonstrated. A system is optimized by two intensity controlled masks, which work in the principle of the Fresnel zone. It is the first time to propose the concept of the pretreatment along the transmission path for solving some serious problems. The numerical simulations of intensity and phase distributions of the RF signals at each key cross-sectional planes of an OAM radio beam are made to prove the optimized effect. And a proof-of-concept experiment at RF 20 GHz demonstrates the feasibility of the system.

As a flexible, tunable, and reconfigurable mean of generating/receiving OAM radio beams, the basic system configuration of OAM based wireless communication employing CAAs is shown in Fig. 1. The antenna elements in the transmitted CAAs are fed with the same radio singles, but with a successive delay from element to element. Such that after a full turn, the phase has been incremented by an integer multiple L of 2π. And they collectively form an OAM radio beam with the topological charge of L. Here, we just give a concept and ignore the phase provided unit, which can be various forms and provides the phase difference among the arrays. The receiving CAAs and the transmitted CAAs are facing each other on the same beam axis in the free space. When the generated OAM beam with the topological charge of L impinges upon the CAAs of the receiver, each element receives an RF signal with a slightly different phase due to the azimuthal phase term $\exp(iL\varphi)$, the properties of the spatial distribution of the OAM radio beam. The phase difference should be compensated, thus the recovered RF signals constructively interfere and form a strong intensity. All of the devices stand along the beam axis.

If this system capacity gain could be calculated as a traditional multiple-in multiple-out (MIMO) communication system by the means of the singular value decomposition and the circulant matrix,[22] the corresponding capacity C_L for known OAM channel at transmitter is described as[23]

$$C_L = \sum_{k=1}^{r} \log_2\left(1 + \frac{P_k}{\sigma_n^2/\mu_k^2}\right) \text{bit/s/Hz}, \tag{1}$$

where r is the rank of the MIMO channel matrix, σ_n^2 is the noise variance on each receiver branch, μ_k is the positive

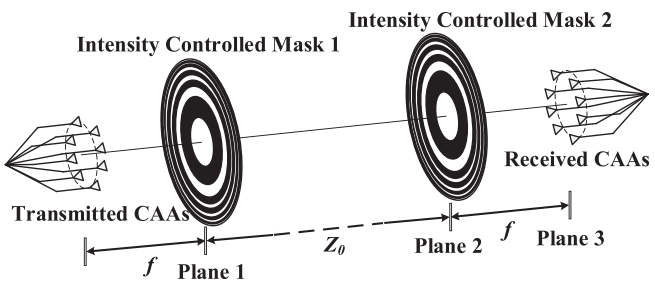

FIG. 1. The proposed schematic configuration of the optimized OAM radio communication system. CAAs: circular array antennas; f: the focal distance of the intensity controlled masks; Z_0: the parallel propagation distance; planes 1, 2, and 3: key cross-sectional planes.

singular values of the diagonal matrix, and all the available power P is distributed across the channels, according to the water-filling principle, such that

$$P = \sum_{k=1}^{r} P_k. \tag{2}$$

The parameters, such as r, σ_n^2, and μ_k, are the same with the traditional MIMO system, but the power P has different features which will effect on the capacity gain deduced by Eq. (1) obviously. The received power P is related to the propagation distance if without any optimized operation. A key distance, the Rayleigh distance d_R for transmitted CAAs, can be defined as

$$d_R = \frac{{D_T}^2}{2\lambda}, \tag{3}$$

where the aperture D_T is set to the transmitting CAAs diameter and λ is the wavelength of RF signals. The OAM beam will perform as follows. Below the Rayleigh distance, the helical phases are not formed but the received power P can be used to get the corresponding capacity gain. When the distance increases above the Rayleigh distance, the clean helical phases can be observed, but the power of all the nonzero OAM channels fall rapidly, and become too weak to be submerged in noise. Another factor to decrease the received power P is about the radius of the receiver CAAs. The radius of the circle of the max-power in the cross-sectional plane is dependent with the topological charge. When two or more topological charge transmitted together, at the situation of OAM-multiplexing, the receiver CAAs just can provide one certain radius, and this means that not all OAM beams are received at each max-power circle. Deduced by Eq. (1), the weak received power P leads to the small capacity gain essentially, and the OAM modes may not achieved an increase in capacity and spectral efficiency.

To solve those fatal issues, we set two intensity controlled masks at the propagation path of OAM radio beams to control the size of the beams to stop the decreasing of the received power P, as shown in Fig. 1. The intensity controlled masks work in the principle of the Fresnel zone, which can work at any frequency and the corresponding lens, Fresnel-zone plate lens (FZPL), can also be used to focus and anti-focus the radio beams.[24] The intensity controlled marks are the simplest FZPL approximately, which is consisting of alternate transparent and reflecting (or absorbing) rings. Moreover, the intensity controlled masks modulate the OAM radio beam's intensity in the radial direction without changing either intensity or phase azimuthal distribution. Thus, the intensity controlled masks has no effects on the key feature of the OAM radio beams. And at the given focal distance f, design wavelength λ, m is the zone number, the Fresnel zone radii are obtained from the following approximate equation:

$$b_m = \sqrt{m\lambda f}. \tag{4}$$

And the two sets of CAAs are placed on the focal planes of the two intensity controlled masks. It is easy to understand

that the size of the OAM radio beam is increasing along with the propagation beam axis, because it is an approximate divergent spherical wave transmitted from the CAAs.[22] The first intensity controlled mask collimates beam from the approximate spherical wave to the approximate plane wave and keeps the beam size unchanging for increasing the propagation distance with small lose. In addition, the second intensity controlled mask does the reverse operation for decreasing the radius difference of the max-power circles of the different OAM mode and enhancing the receiving power P.

In addition, the field radiated by the CAAs is the superposition of specific and infinite OAM modes.[20] Although the expected OAM mode is the main component, the redundant components needs to be blocked. As it is known that the radius of the circle of the linear momentum max power in the cross-sectional plane increases along with the increasing of the absolute value of the topological charge. Thus, only the expected OAM mode with minimum radius will be collimated by the intensity controlled mask with certain and limited area. While the redundant modes will be filtered away.

Fig. 2 shows the simulated intensity and phase distributions of OAM radio beam with the topological charge $L = 3$ at 20 GHz. The numerical simulated conditions are $f_{RF} = 20$ GHz, $N = 16$, $D_T = 6$ cm, $f = 60$ cm, and $Z_0 = 240$ cm, and the observed range is ± 40 cm. The patterns at the first, second, and third rows in Fig. 2 show the characteristics of electromagnetic field at key planes upon propagation, plane 1, plane 2, and plane 3 in Fig. 1, respectively. Figs. 2(a)–2(c) stand for the 2D intensity distributions, in normalized units being proportional to square of amplitude, from blue to yellow representing from low to high. And they present a typical shape of an OAM radio beam, which is a bright ring with no intensity at the center. Figs. 2(d)–2(f) describe the 2D phase distributions. The number of twists indicates the magnitude of the charge, and the twist direction implies the sign of the change. Thus, the features of Figs. 2(d)–2(f) testify that the topological charge of the OAM radio beam is keeping as $L = 3$. Moreover, the characteristics of OAM radio beam are mainly reflected in continuous phase change in the azimuthal direction, while the operations are all in the radial direction. Thus, the intensity controlled masks do not destroy the features of the OAM radio beam. In order to show optimized results clearly, Figs. 2(g)–2(i) depict the 1D intensity curves at the black dotted line in Figs. 2(a)–2(c) and 2(j)–2(l) show the 1D phase curve mapping to Figs. 2(d)–2(f). The radio beam was transmitted to the plane 1 freely with the propagation distance as long as 5 times the Rayleigh distance d_R. Calculated by Eq. (3), d_R is 12 cm at this simulated conditions. After modulated by the intensity controlled mask 1, the OAM radio beam propagates 20 times d_R. Figs. 2(g) and 2(h) show the size of beam is almost constant and Figs. 2(g)–2(i) are in normalized units at the max value in Fig. 2(g). Although a part of energy is lost due to the reflecting (or absorbing) rings of the mask, the max values of Figs. 2(g) and 2(h) only has a small loss with the value of -4.8 dB. Except the micro-region around phase singular point, the phase curve has a slow change in Fig. 2(k) in sharp contrast to the performance in Fig. 2(j). Thus, even under the condition of removing the intensity controlled mask 2, the OAM radio beam is easy to be received. The beam size is small as the diameter of the received and the transmitted CAAs and the power is very high in Fig. 2(j) with the value of 9.1 dB. The total propagation distance is 360 cm, which is 30 times d_R.

The experimental setup is schematically introduced and shown in Fig. 3(a), which can be considered as a transmitter,

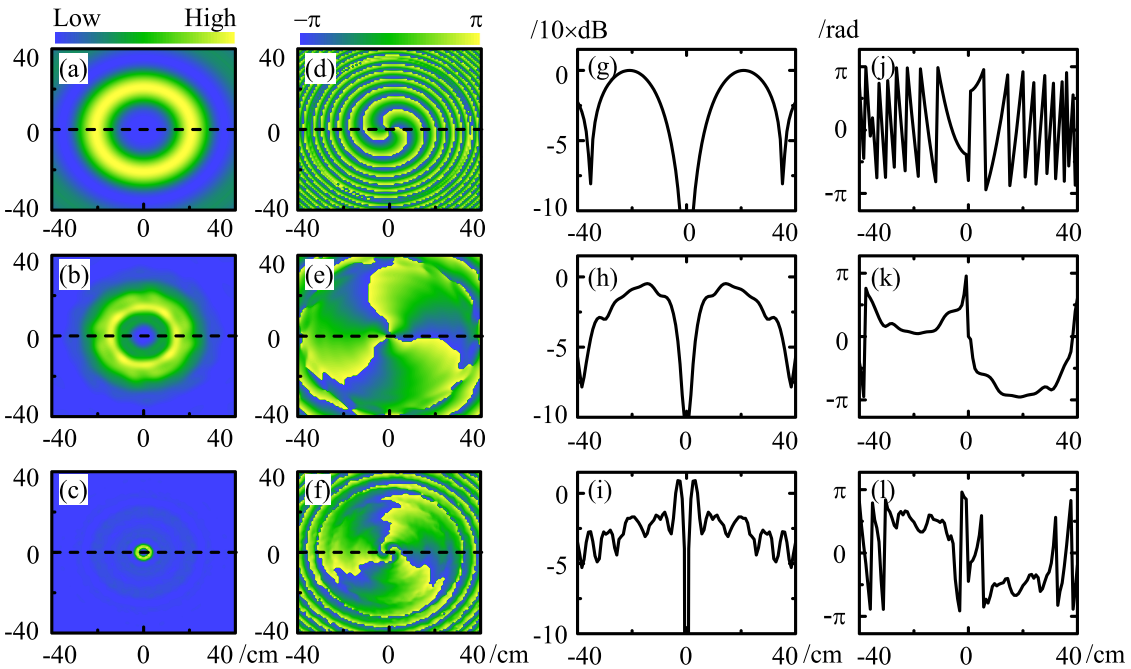

FIG. 2. Calculated intensity and phase distributions of the OAM radio beam ($L = 3$) on the key planes upon propagation. The patterns at the first, second, and third rows show the characteristics of electromagnetic field at plane 1, plane 2, and plane 3 (in Fig. 1), respectively. (a)–(c): 2D intensity distributions (in arbitrary units); (d)–(f): 2D phase distributions; (g)–(i): the 1D intensity curve at the black dotted line in (a)–(c) (in normalized units at the max value in (g)/10 × dB); (j)–(l) the 1D phase curve at the black dotted line in (d)–(f). $f_{RF} = 20$ GHz, $N = 16$, $D_T = 6$ cm, $f = 60$ cm, and $Z_0 = 240$ cm. The observed range is ± 40 cm.

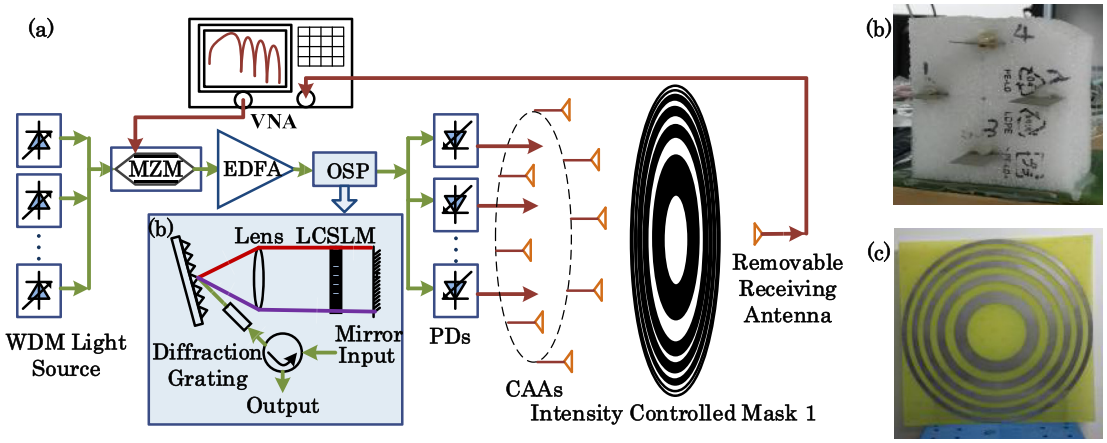

FIG. 3. (a) Experimental setup of the OAM radio beam collimating by the intensity controlled mask. (b) Photograph of the real array antennas with four elements. (c) Photograph of the real intensity controlled mask. VNA: vector network analyzer; WDM: wavelength-division multiplexing; MZM: Mach-Zehnder modulator; EDFA: erbium-doped fiber amplifier; OSP: optical spectrum processor; PDs: photoelectric detectors; and LCSLM: liquid crystal spatial light modulator.

optimizer and survey meter for an OAM radio beam with topology charge $L = 3$ at frequency of 20 GHz. This experiment arms at measuring the characteristics of electromagnetic fields of the generated OAM radio beam at planes of different propagation distances. The phase provided unit of the transmitter, which can be various forms and provides the phase difference among the elements of the transmitted CAAs, is the same phase provided unit of one reference based on microwave photons technology.[20] The photograph of the real array antennas with four elements used in the experiment is shown in Fig. 3(b). The array element is a kind of custom-made patch antenna, and the diameter is equal to 6 cm. In this proof-of-concept experiment, only an intensity controlled mask is employed as the optimizer, and its photograph is shown in Fig. 3(c). The realistic mask is created by controlling a printed circuit board router to drill the required shapes on copper plate with the size 60 cm × 60cm. The focal distance of the intensity controlled mask is 60 cm, and the frequency of the OAM radio beam is 20 GHz. According to Eq. (4), the Fresnel zone radii are 9.49 cm, 13.42 cm, 16.43 cm, 18.97 cm, 21.31 cm, 23.24 cm, 25.10 cm, 26.83 cm, 26.46 cm, and 30.00 cm, sequentially. A removable receiving patch antenna, as the probe survey meter, is controlled by a stepper motor and routes along a straight line which is perpendicular to the propagation direction and pass through the field center. And then the electromagnetic field characteristic of OAM radio beams along the route is measured by the high precision vector network analyzer (VNA). And the experimental process is programmable and distant controlled.

The experimental results of the OAM radio beam's electromagnetic characteristic at different propagation distances are shown in Fig. 4. Figs. 4(a)–4(c) are the experimental power curves of OAM radio beam for Z = 30 cm, Z = 40 cm, and Z = 60 cm with any operation, orderly. The beam size is increasing and the power is decreasing rapidly with the propagation distance, the max-power values of the three curves are −46.59 dbm, −49.15 dBm, and −53.09 dbm, respectively. Figs. 4(d) and 4(e) are the OAM radio beam's electromagnetic characteristics at Z = 60+240 cm, 200 times of wavelength, after being optimized by the intensity controlled mask 1 and propagating with distance of 240 cm. In Fig. 4(d), the negligible intensity is observed near the center, which is almost the experiment noise value −80 dBm, and the beam size is similar to it in Fig. 4(c). The max power is −54.82 dBm, and is smaller than Fig. 4(c) with 1.73 dBm. The optimized results are obvious and effective. The one-dimensional (1D) measured phase curve shown in Fig. 4(e) presents phase characteristic of an OAM radio beam. When the 1D phase curve crosses the center, a sharp variation with

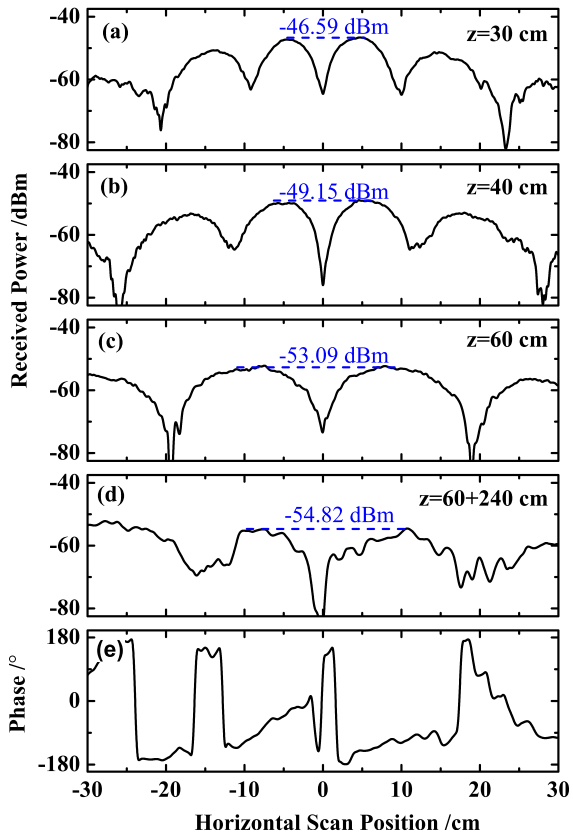

FIG. 4. (a)–(d) Experimental power curves of the generated OAM radio beam L = 1 at different propagation distances. (a)–(d): Z = 30 cm, Z = 40 cm, Z = 60 cm, and Z = 60+240 cm (optimized). (e) Measured phase curve of the OAM radio beam L = 1 at the same propagation distance with (d).

an approximate value of 180° appears. This fits the feature of the OAM radio beam with charge $L = 1$, theoretically. In addition, all the measured phase values are expressed in the range from −180° to 180°. Furthermore, when the phase curve passes the 180° or −180°, a leap appears. So, there are several leaps on the phase curve.

In this paper, the OAM-based wireless communication system is optimized by two intensity controlled masks, which work along the principle axis of the Fresnel zone. The numerical simulations of intensity and phase distributions of the RF signals at each key cross-sectional planes of an OAM radio beam are made to prove the optimized effect. Moreover, the experimental results measured at 200 times of wavelength (300 cm) are the best performances of OAM radio beams at 20 GHz presented in references so far. And the feasible system with the concept of the pretreatment along the transmission path may pave the way to the practical OAM based applications such as exploration in astrophysics, high spectral efficiency wireless communication, and privacy communication system.

This work is supported in part by the National Basic Research Program of China (973 Program) (No. 2012CB315604), the NSFC (Nos. 61205058 and 61331008), the Hi-Tech Research and Development Program of China (863 Program) (No. 2012AA011302), the Program for New Century Excellent Talents in University (NCET-12- 0793), the Beijing Nova Program (No. 2011065), and the Open Fund of IPOC (BUPT).

[1]L. Allen, M. W. Beijersbergen, R. J. C. Spreeuw, and J. P. Woerdman, Phys. Rev. A **45**, 8185 (1992).
[2]A. M. Yao and M. J. Padgett, Adv. Opt. Photonics **3**, 161 (2011).
[3]G. Gibson, J. Courtial, and M. J. Padgett, Opt. Express **12**, 5448 (2004).
[4]J. Wang, J. Yang, I. M. Fazal, N. Ahmed, Y. Yan, H. Huang, Y. Ren, Y. Yue, S. Dolinar, M. Tur, and A. E. Willner, Nat. Photonics **6**, 488 (2012).
[5]C. Guo, S. Yue, and G. Wei, Appl. Phys. Lett. **94**, 231104 (2009).
[6]E. Karimi, B. Piccirillo, E. Nagali, L. Marrucci, and E. Santamato, Appl. Phys. Lett. **94**, 231124 (2009).
[7]Y. Ren, H. Huang, G. Xie, N. Ahmed, Y. Yan, B. I. Erkmen, N. Chandrasekaran, M. P. J. Lavery, N. K. Steinhoff, M. Tur, S. Dolinar, M. Neifeld, M. J. Padgett, R. W. Boyd, J. H. Shapiro, and A. E. Willner, Opt. Lett. **38**, 4062 (2013).
[8]Y. Yan, Y. Yue, H. Huang, Y. Ren, N. Ahmed, M. Tur, S. Dolinar, and A. Willner, Opt. Lett. **38**, 3930 (2013).
[9]F. Tamburini, E. Mari, A. Sponselli, B. Thidé, A. Bianchini, and F. Romanato, New J. Phys. **14**, 033001 (2012).
[10]F. Tamburini, E. Mari, B. Thidé, C. Barbieri, and F. Romanato, Appl. Phys. Lett. **99**, 204102 (2011).
[11]M. Tamagnone, C. Craeye, and J. Perruisseau-Carrier, New J. Phys. **15**, 078001 (2013).
[12]F. Tamburini, B. Thidé, E. Mari, A. Sponselli, A. Bianchini, and F. Romanato, New J. Phys. **14**, 118002 (2012).
[13]B. Thidé, H. Then, J. Sjöholm, K. Palmer, J. Bergman, T. D. Carozzi, Y. N. Istomin, N. H. Ibragimov, and R. Khamitova, Phys. Rev. Lett. **99**, 087701 (2007).
[14]S. M. Mohammadi, L. K. S. Daldorff, J. E. S. Bergman, R. L. Karlsson, B. Thidé, K. Forozesh, and T. D. Carozzi, IEEE Trans. Antennas Propag. **58**, 565 (2010).
[15]X. Gao, S. Huang, J. Zhou, Y. Wei, C. Gao, X. Zhang, and W. Gu, J. Opt. **15**, 105401 (2013).
[16]J. Yao, J. Lightwave Technol. **27**, 314 (2009).
[17]Z. Cao, R. Lu, Q. Wang, N. Tessema, Y. Jiao, H. P. A. van den Boom, E. Tangdiongga, and A. M. J. Koonen, Opt. Lett. **39**, 3402 (2014).
[18]X. Yi, L. Li, T. X. H. Huang, and R. A. Minasian, Opt. Lett. **37**, 608 (2012).
[19]Y. Song, S. Li, X. Zheng, H. Zhang, and B. Zhou, Opt. Lett. **38**, 3245 (2013).
[20]X. Gao, S. Huang, Y. Song, S. Li, Y. Wei, J. Zhou, X. Zheng, H. Zhang, and W. Gu, Opt. Lett. **39**, 2652 (2014).
[21]F. Bian, S. Li, Y. Song, Q. Yu, X. Gao, X. Zheng, H. Zhang, and B. Zhou, paper presented at CLEO: QELS Fundamental Science, San Jose, CA, 8–13 June 2014, paper JW2A.15.
[22]O. Edfors and A. J. Johansson, IEEE Trans. Antennas Propag. **60**, 1126 (2012).
[23]I. E. Telatar, Eur. Trans. Telecommun. **10**, 585 (1999).
[24]H. D. Hristov and M. H. A. J. Herben, IEEE Trans. Microwave Theory Tech. **43**, 2779 (1995).